J Mater Sci: Mater Med (2009) 20:959–965
DOI 10.1007/s10856-008-3651-7

Ultrastructural observation of electron irradiation damage of lamellar bone

S. I. Hong · S. K. Hong · J. M. Wallace · D. H. Kohn

Received: 22 May 2008 / Accepted: 3 November 2008 / Published online: 26 November 2008

Abstract The ultrastructure of murine femoral lamellar bone and the effect of electron irradiation (200 kV) on collagen and mineral features were investigated using in situ high resolution transmission electron microscopy (HRTEM). Bands of collagen fibrils were mostly aligned parallel to the long axis of the bones, with some bands of fibrils inclined in longitudinal sections. The similarity of the ultrastructure between the longitudinal and transverse sections supports the rotated plywood structure of the lamellar bone. The collagen fibrils appeared damaged and the mineral crystals were coarsened after electron irradiation. Continuous diffraction rings became spotty and the contrast between rings and the background became sharper, further suggesting coarsening of apatite crystals and increased crystallinity after irradiation. No new phases were observed after irradiation. Both the damage to collagen and coarsening of apatite crystals can deteriorate the strength and integrity of bone, and may provide insight into fracture in patients who have undergone radiation therapy.

S. I. Hong · D. H. Kohn
Department of Biologic and Materials Sciences, University of Michigan, Ann Arbor, MI 48109-1078, USA

S. I. Hong (✉)
Department of Nano-materials Engineering, Chungnam National University, Taejon 305-764, South Korea
e-mail: sihong@cnu.ac.kr

S. K. Hong
Department of Materials Science and Engineering, Chungnam National University, Taejon 305-764, South Korea

J. M. Wallace · D. H. Kohn
Department of Biomedical Engineering, University of Michigan, Ann Arbor, MI 48109-2099, USA

1 Introduction

The deleterious effect of high energy radiation on the integrity of human bone is well documented although its cause is not fully understood [1, 2]. For example, osteopenia and osteoporosis in the survivors of childhood cancer have been linked to irradiation treatments [3, 4]. High dose local radiation therapy in adults also causes atrophy of the trabeculae of bone [1, 5], i.e. osteoporosis, particularly after kilo-voltage doses of irradiation. It is not clear, however, whether the loss of bone mass is caused by a direct effect of the radiation or an indirect effect, such as a reduction of growth hormone secretion by radiation [6]. Regardless of the mechanism, spontaneous fractures after irradiation have been attributed to the loss of bone mass, which is typically detected radiographically [5]. In a more recent study, no significant differences in bone mineral content were observed between irradiated and matched control patients 1–7 years after radiotherapy [7]. Hopewell [1] therefore suggested that the susceptibility to fracture after radiotherapy could occur without a change in bone mineral content. One possibility is a change in the integrity of collagen fibrils and mineral apatite induced by radiation, without a change in bone mineral content or bone mass (i.e. a change in bone quality). A precedent of alterations in collagen and mineral without changes in bone mass exists in exercise models of bone adaptation [8].

The nanostructural observation of live or even dead bulk bone under irradiation to study irradiation damage at the nanoscale in real-time is technically impossible. Even though it is hypothesized that the nanostructure of bone can be modified by irradiation, the difficulty and high cost involved even in destructive analysis of bone after radiation exposure have made sub-microstructural analyses scarce. Therefore, the evolution of the nanostructure of

apatite and collagen fibrils under irradiation and what nanostructural changes can occur in the absence of changes in bone mineral content are unknown. Observations of materials under irradiation in the transmission electron microscope (TEM) are useful because they provide insight into nanostructural and phase changes in thin sections under irradiation [9–12]. TEM observations of dehydrated fixed thin bone samples could therefore suggest mechanisms of apatite crystal and collagen fibril changes under irradiation. Since even post-irradiation TEM observations of bone, let alone in situ nanostructural observations of bulk bone are not available at present, observations of samples irradiated in the TEM can be a cost-effective and convenient first step toward direct analyses of sub-microstructural evolution of apatite during irradiation at high energy levels. Irradiation in the TEM provides insights into bulk behavior, although some caution should be exercised in applying thin film behavior to bulk behavior.

Local crystalline changes and phase transformations secondary to irradiation have been observed in synthetic apatite compounds in TEM [9, 10]. For example, small voids form after a low beam current irradiation (1.6 A/cm^2) and CaO precipitates from apatite after a high beam current irradiation (16 A/cm^2) [10]. The direct observation of irradiation damage in biological apatite using TEM has been made on thin human dental enamel [11], which exhibited mass loss due to the formation of voids and beam-induced phase transformation of apatite to CaO. In this study, murine femoral lamellar bone was observed in the TEM to investigate the effect of high kilo-voltage electron irradiation on the sub-microstructural evolution. The main objective of this study was to investigate the effects of irradiation on the ultrastructure of thin plastic-imbedded bone samples. In situ nanostructural observations of bone during irradiation in the TEM provide insight into local changes in mineral and collagen under high energy irradiation of doses equivalent to those used clinically.

2 Experimental methods

Femora ($N = 3$) were extracted from male C57BL/6 mice aged 12 months (University of Michigan UCUCA approval #8518), and the soft tissue was carefully stripped off. Transverse (perpendicular to the long bone axis) and longitudinal (parallel to the long bone axis) sections were obtained from the midshafts of femora by cutting with a low speed saw with calcium buffered saline solution as a lubricant and coolant. Bone specimens were fixed in Sorenson's buffer with 2.5% glutaraldehyde, postfixed in 1% osmium tetroxide and dehydrated in an ethanol series (30, 50, 70, 90, 100%) and acetone (100%). Specimens were then infiltrated with a series of graded mixtures of acetone and Spurr resin and embedded in fresh Spurr resin in Beem capsules. Embedded samples were polymerized at 65°C for 24 h. Ultrathin sections (60–70 nm) of lamellar bone were cut parallel and perpendicular to the axis of the long bone ($\sim$60 sections each) with a diamond knife on a MIL ultramicrotome and picked up on 300-mesh Cu grids.

High resolution transmission electron microscope (HRTEM) observations were carried out using a JEOL JEM2010 electron microscope operated at 200 kV. In order to determine the crystal structure of the mineral, selected area electron diffraction (SAED) was performed. In order to observe the effect of electron irradiation on the ultrastructure of lamellar bone, some samples ($N = 1$ grid/bone; 1 grid has 6–7 sections) were exposed to electron irradiation (at 200 kV) for 10 min before photographing and SAED analyses. Control micrographs were taken within 100 s. of exposure to irradiation.

The in situ irradiation/TEM technique employed is a routine technique, in which a sample stays in the TEM and structural evolution is observed with time [12]. Irradiation in the TEM is therefore a convenient and cost-effective method for obtaining insight into the effects of irradiation on the ultrastructure of bone. The current density during observation in the TEM was 15–30 pA/cm^2, depending on the magnification (the higher the magnification, the smaller the current density). If the average current density is 20 pA/cm^2 and the exposure time is 10 min, the absorbed dose is calculated to be 0.36 Gy, which converts to 0.36 Sv assuming the radiation weighting factor W_R is 1 (W_R is 1 for X-rays, gamma rays and β particles). The dose in control specimens was $\sim$0.06 Sv assuming the observation time was 100 s.

3 Results and discussion

The longitudinal sections of the femora (Fig. 1a) displayed well-aligned and uniformly distributed collagen fibrils mostly parallel to the long axis of the bone (indicated by the black arrow). The collagen fibrils were tightly packed in parallel, to accommodate the tensile stress along their axis [13]. In some regions, bands of collagen fibrils inclined with respect to the long axis were observed (marked with white circles). The angles between the inclined collagen fibrils and the axis were 30–70 degrees. The presence of inclined collagen fibrils supports the rotated plywood structure model of lamellar bone [14, 15].

Apatite crystals (marked with white arrowheads) appeared thicker than the collagen fibrils, similar to previous TEM observations of bone [15, 16]. The edges of the apatite crystals were mostly being viewed in Fig. 1a. The selected area diffraction pattern (Fig. 1b) from the area

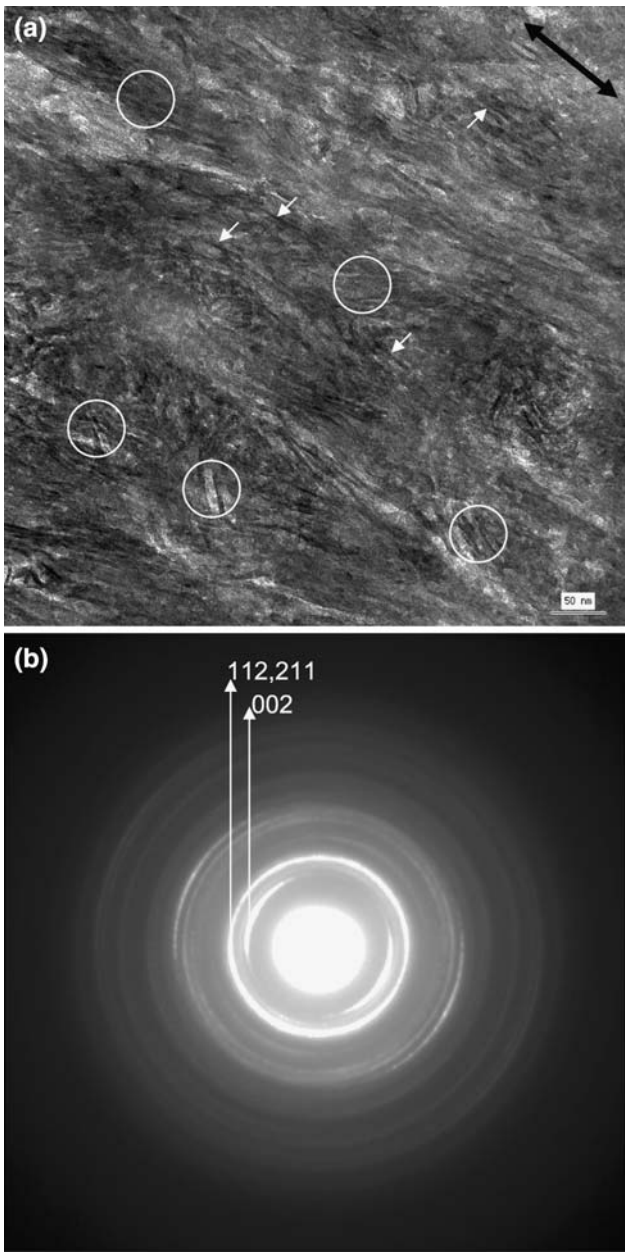

Fig. 1 **a** Representative HRTEM image of a longitudinal section of femoral lamellar bone. Bands of parallel collagen fibrils are mostly parallel to the long axis of the bone (indicated by a black arrow), with some bands inclined at an angle to the long axis (circled). Apatite crystals (white arrowheads) appear thicker than the collagen fibrils. **b** Selected area diffraction pattern from the area shown in **a** exhibited continuous (121) and (211) rings and strong and wide (002) arcs

shown in Fig. 1a exhibited strong (002) arcs, supporting the presence of collagen fibrils parallel to and inclined with respect to the axis. In the longitudinal section, the (002) ring is one of the strongest, suggesting that the c-axes of the apatite crystals were mostly parallel to the longitudinal plane of the long bone. In Fig. 1b, the two strongest rings are indexed. The spacing between the (112) and (211) planes is so close that the rings can't be separated in the diffraction pattern.

In the transverse sections (Fig. 2a), bands of parallel collagen fibrils were also observed. The collagen fibrils, however, were shorter and less well-aligned compared to those of the longitudinal sections. The appearance of bands of collagen fibrils in the transverse direction, as opposed to

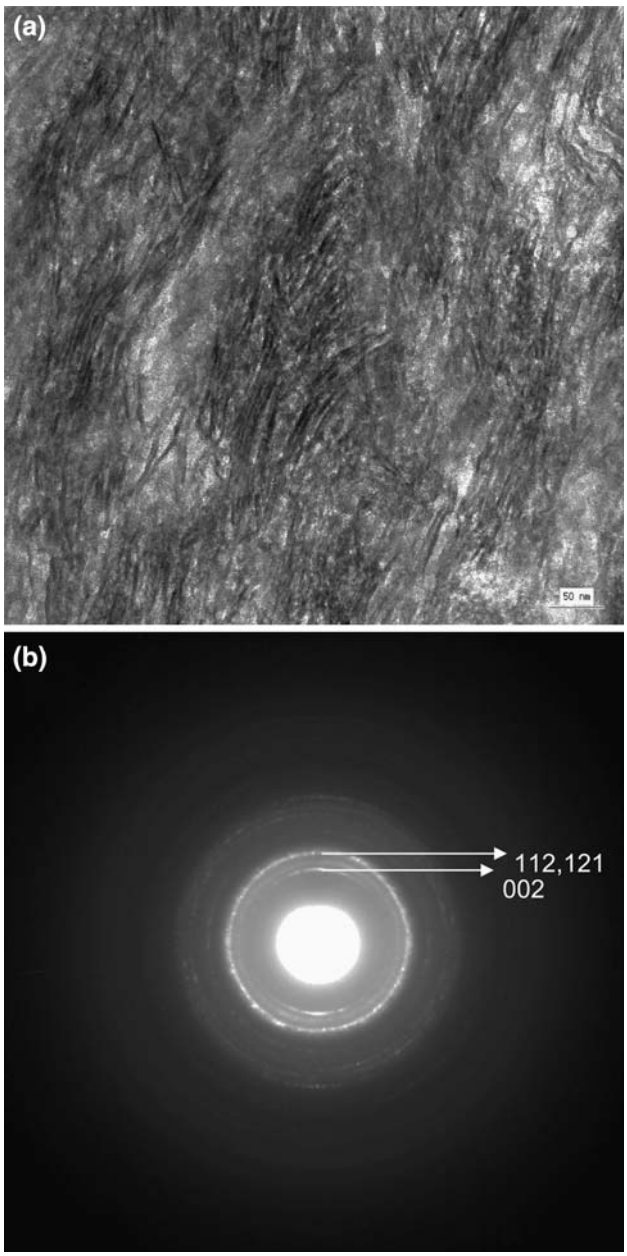

Fig. 2 **a** Representative HRTEM image of a transverse section of femoral lamellar bone. The collagen fibrils were shorter and less well-aligned compared to those of the longitudinal sections (Fig. 1a), but the transverse and longitudinal sections of lamellar bone have a similar appearance in support of the rotated plywood structure. **b** Selected area diffraction patterns were weaker than those of the longitudinal sections (Fig. 1b), suggesting a lower planar density of apatite crystals in the transverse sections

just observations of fibril cross-sections, is consistent with the observation of Mariotti [17] using SEM (scanning electron microscopy) that the transverse and longitudinal sections of lamellar bone have a similar appearance due to the rotation of collagen fibril arrays [15].

Transverse fracture surfaces are similar to longitudinal fracture surfaces [14, 18]. The similarity in fracture morphology results from the variation of collagen fibril orientation between lamellae, as suggested in the rotated plywood structure [15]. Ascenzi and Bonucci [19] and Reid [20] suggested that fibrils are parallel to the interlamellar boundaries and that fibril directions are nearly orthogonal to each other in adjacent lamellae. Ascenzi and Benvenuti [21] also observed criss-crossed oblique collagen fibrils in the transition zone between adjacent lamellae with orthogonal fibrils. Collectively, these observations are consistent with our findings of bands of collagen fibrils in both longitudinal and transverse sections. The observation that collagen fibrils are longer and better-aligned in longitudinal sections suggests that there are more collagen fibrils oriented in this direction.

The diffraction patterns (Fig. 2b) from the transverse sections shown in Fig. 2a were weaker than from the longitudinal sections (Fig. 1b), suggesting that the planar density of apatite crystals in the longitudinal section is higher. The size of apatite crystals in human bone is ~50 nm (length) × ~25 nm (width) × ~10 nm (thickness) with the length parallel to the *c*-axis [22]. The stronger diffraction pattern in the longitudinal sections also suggests that a larger population of crystals was aligned with the *c*-axis parallel to the long axis of the bones. Since the crystals are aligned such that their c-axes are parallel to the length of the collagen fibrils [14], the diffraction results also indicate that a significant fraction of collagen fibrils were parallel to the long axis, despite the rotated plywood structure of lamellar bone.

A representative region with two prominent orientations of cross-hatched collagen fibrils (enclosed by a white circle) just after exposure to electron irradiation and after 10 min of electron irradiation is shown in Fig. 3a, b, respectively. The crystals marked with white arrows and denoted a–e indicate the same crystals before and after irradiation. The orientation difference between the two sets of collagen fibrils in Fig. 3a, b is 35–40°, which is compatible with the observations of other investigators [14, 15].

One significant observation is the gradual ultrastructural change that took place during electron irradiation in the microscope. After 10 min of irradiation, the collagen fibrils were no longer visible (Fig. 3b), suggesting that the structure of the fibrils was damaged by electron irradiation. Detailed information on ultrastructural damage of collagen fibrils could not be obtained because the phase contrast of

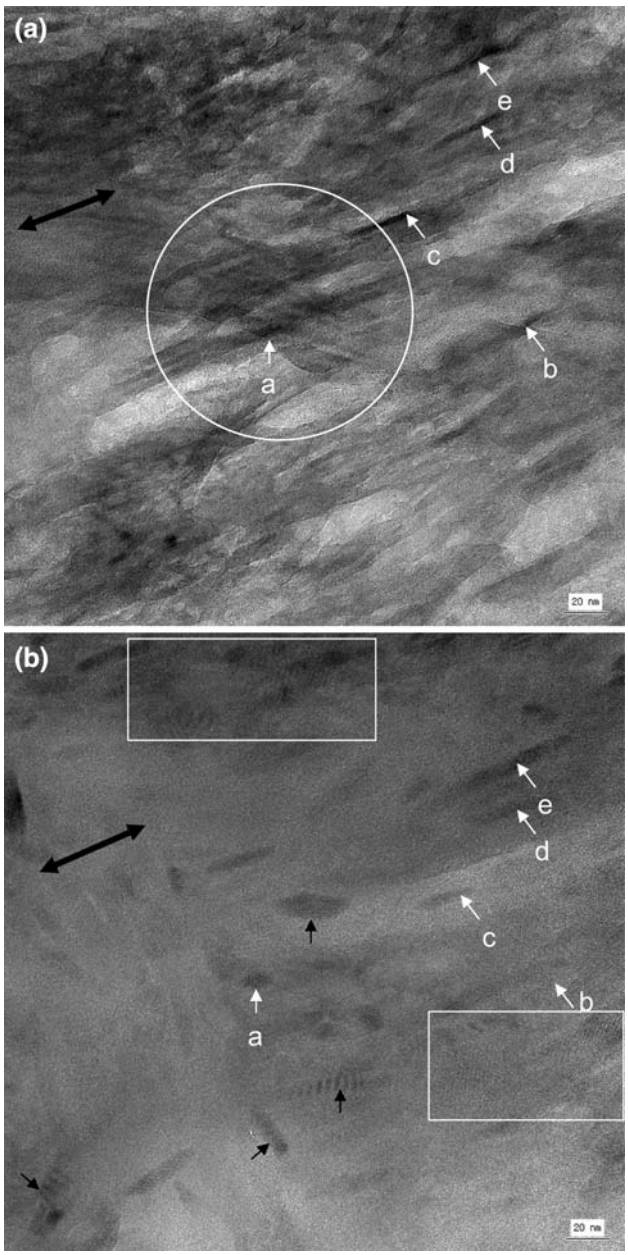

Fig. 3 A region with two prominent orientations of collagen fibrils (white circle) just after exposure to electron irradiation (**a**) and after 10 min of electron irradiation (**b**). Ultrastructural changes took place under electron irradiation in the microscope. Collagen fibrils degraded, but apatite crystals were still visible induced by irradiation. Crystals marked with white arrows and denoted a–e indicate the same crystals before and after irradiation and show alterations in size, reflective of crystallization. Lattice fringes became larger and sharper in contrast with irradiation, (white rectangles), indicating coarsening of apatite crystals. The orientation of some crystals (marked by small black arrows) differed from the original orientation of the fibrils and may be newly nucleated crystals

the collagen disappeared under irradiation, but the crystalline apatite could be observed. Gamma-irradiation cleaves the peptide bonds in collagenous materials [23–25]. The cleavage of peptide bonds in collagen may reduce its

strength and expedite its degradation. The mechanical properties of irradiated cortical bone are also affected by the destruction or deterioration of collagen fibrils [25, 26]. Our findings therefore suggest that the model of electron irradiation used in this study is consistent with other models of collagen degradation and may provide an ultrastructural basis for irradiation-induced fragility.

Another interesting observation was the coarsening and increased contrast and visibility of apatite crystals. The area with the lattice fringes (enclosed by rectangles in Fig. 3b) became bigger and sharper in contrast, suggesting that the crystallinity and size of some of the apatite crystals increased. In Fig. 3, crystals marked with "a", "b", "c", "d" and "e" indicate the same crystals before and after irradiation. The long axes of most apatite crystals were still parallel to the original orientation of collagen fibrils, suggesting that some crystals grew at the expense of others. For example, the crystals marked "c" and "d" became smaller, whereas the crystal marked "e" became larger. Some crystals whose orientations were different from the original orientation of the fibrils (marked with black arrows) may be newly nucleated and grown crystals induced by electron irradiation.

The selected area diffraction patterns taken from the same area shown in Fig. 3 before (4a) and after 10 min of irradiation (4b) exhibited several differences. First, the contrast between diffraction rings and the background became sharper after irradiation, suggesting more crystal perfection and increased crystallinity. Second, the (003) ring which was not clear before irradiation because it was too close to the diffuse (112) ring was distinct after irradiation as the (112) ring became sharper, also suggesting increased crystallinity after irradiation. Third, the continuous rings became spotty rings, suggesting the misorientation angle between crystals increased. The misorientation angle increases either because the orientation of crystals changes without modification in size, or because some crystals coarsen at the expense of others so that the number of crystals decreases. The presence of larger sized apatite in Fig. 3, along with the spotty rings in Fig. 4 suggest that the latter mechanism is operative and crystallization (increasing crystalline/amorphous ratio) and growth of bone mineral took place under irradiation. It should be noted, however, that no new rings appeared after irradiation and the indices of all rings and spots matched with those before irradiation and matched those of hydroxyapatite (Fig. 4). These findings suggest that just the misorientation angle increased, but no phase transformations occurred and no new phases were formed after irradiation, unlike in natural apatite minerals, where CaO can form [9, 10].

To our knowledge, this is the first detailed study of the effect of high energy irradiation on lamellar bone at the sub-micron scale. However, there are several reports on the effect of irradiation on human dentin and enamel [11, 27, 28], and synthetic [9] and natural apatite [10]. Bres et al. [11] observed mass loss due to the formation of voids and electron beam-induced phase transformation to CaO in HRTEM at 300–400 kV, which is higher than that (200 kV) used in this study. Lin et al. [27] studied the effect of CO_2 laser irradiation on the structure of human enamel and dentin and observed a new small XRD (X-ray

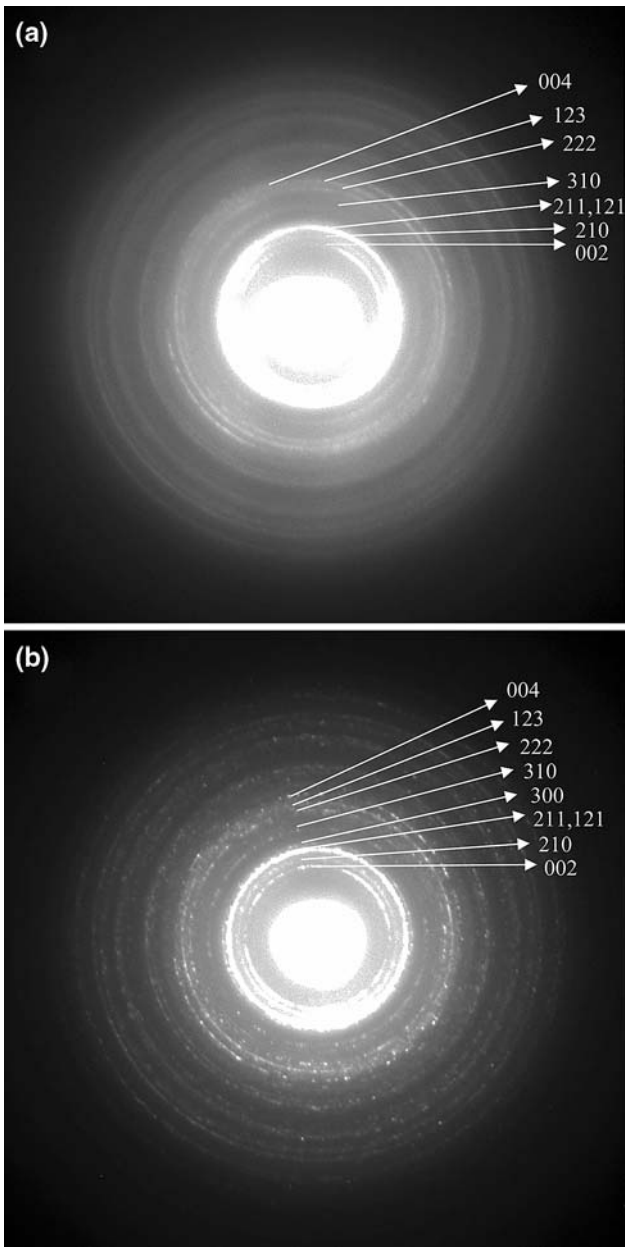

Fig. 4 Selected area diffraction patterns taken from the same area shown in Fig. 3 before (a) and after 10 minutes' irradiation (b). The contrast between diffraction rings and the background became much sharper after 10 minutes' irradiation, and the continuous rings became spotty rings, suggesting more perfection to crystallinity and the increased misorientation angle between crystals

diffraction) peak at the position of $2\theta = 30.78°$ belonging to α-TCP. Lin et al. [27] also observed sharper peaks on the X-ray diffraction patterns of enamel after CO_2 irradiation and attributed it to the grain growth and increased crystallinity. Lin et al. [27], however, did not observe the ultrastructure to confirm grain growth. Watary [28] observed coarsening of the ultrastructure after CO_2 irradiation using AFM (atomic force microscopy) and suggested that apatite crystals grew to the size of several hundreds nm from the initial size of 50–150 nm.

The coarsening of apatite crystals and increased crystallinity observed in the present study are consistent with the observations in dentin and enamel under CO_2 irradiation [27]. However, no phase changes or formation of CaO were observed. The absence of a phase transition in bone under TEM may be attributed to the differences in crystal content and structure between bone and dentin and the higher temperature attained during CO_2 irradiation [27]. Lin et al. [27] and Watary [28] observed local melting of the enamel and suggested that the local temperature could rise over 1000°C. The temperature rise in TEM is less than 10 K [29] because the chamber around the sample is cooled with liquid nitrogen. It should also be noted that the accelerating voltage (200 kV) used in the present study is lower than that (300–400 kV) used by Bres et al. [11], ensuring a lower temperature rise.

The interface energy to volume free energy ratio is higher with smaller crystals. In bone, the crystal size is regulated by the collagen structure since the crystals are nucleated in the collagen hole zone [30]. Since the structure of collagen is damaged under irradiation [25], the interface between the collagen and the crystals is likely to be damaged by irradiation, resulting in an increase in interface energy. The apatite is free to grow upon collagen being degraded by irradiation since this relaxes the crystals and relieves residual stress. A reduction in total interface energy of the system can be achieved by the growth of the crystals because the interface energy to the volume free energy ratio decreases with growth of apatite crystals. Smaller or irregular-shaped apatite crystals with higher interface energy are likely to be degraded under electron irradiation, providing a source of ions to the growing crystals. Ions eluted from damaged crystals with higher interface energy diffuse along the collagen fibrils and attach to the growing crystals, lowering the total energy of the system. The structural disintegration of collagen during irradiation may also facilitate the diffusion of ions.

Irradiation studies in the TEM have been employed in the materials field extensively because the technique is convenient, cost-effective and provides useful information about ultrastructural changes in materials under irradiation [9–12, 31]. Nonetheless, caution should be exercised in applying the observations of this study to damage in live bone. The irradiation dose levels during TEM observation and radiation therapy and diagnosis will be briefly compared, so the readers can understand the intensity of radiation between these different techniques. Our intention is not to model CT imaging or any other type of in vivo irradiation based on observation of thin TEM specimens, but to present the dose used in TEM and doses of some clinical techniques that use irradiation for therapy and diagnosis, so the reader can understand the similarities and differences between the various techniques.

The energy level and time of exposure during irradiation of bone in the TEM are different from radiation therapy, and a direct association between the two cases is not always appropriate. The radiation dose on the irradiated specimens was 360 mSv and that on the control specimens was 60 mSv, as explained in the Experimental Methods. This dose is higher than the dose ($\sim$10 mSv) experienced during computed tomography (CT), but much lower than the daily dose in radiation therapy for cancer ($1–2 \times 10^3$ mSv) [32, 33]. No radiation damage of the bone is expected during CT, and no microstructural change was observed in control specimens (e.g. Fig. 3). The average person receives an effective dose of about 3 mSv per year from naturally occurring radioactive materials and cosmic radiation from outer space. In certain high background radiation areas, such as Guarapari, Brazil and Ramsar, Iran, people receive 200–300 mSv per year [34]. Acute radiation exposure up to 500–1000 mSv causes low-level radiation sickness. Short-term radiation at high doses is more hazardous because damage processes exceed the capacity of tissue to heal.

The bone samples prepared for TEM underwent various procedures, including dehydration, fixing, embedding and polymerization, and may behave differently from live bone, although the mineral behavior is not likely affected by the TEM specimen preparation procedure [35]. Another possible criticism of this method is that thin film behavior could be different from bulk behavior. Despite these shortcomings, irradiation in the TEM is a convenient and cost-effective method for obtaining insight into the effects of irradiation on the ultrastructure of bone, and more precise and detailed ultrastructural observations of bone under irradiation can be a new area of investigation.

4 Conclusions

The effect of electron irradiation on the ultrastructure of bone was investigated. TEM samples were prepared from the midshaft of murine femora and observed using a high resolution transmission electron microscope (HRTEM). Collagen fibrils were well-aligned and uniformly distributed with some bands of inclined fibrils in longitudinal

sections. Collagen fibrils exhibited a similar appearance in transverse sections, though they were shorter and less well-aligned, supporting the rotated plywood structure of lamellar bone. Damage of collagen fibrils and coarsening of crystalline apatites were induced by electron irradiation at 200 kV. The continuous diffraction rings became spotty and the contrast between rings and the background became sharper, supporting coarsening of crystals and increased crystallinity after irradiation. No new diffraction rings and spots were observed, suggesting no new phase formation after electron irradiation. The observations of irradiation induced collagen degradation and coarsening of bone mineral apatite indicates that the integrity and load carrying capacity of bones can be degraded through exposure to irradiation since coarsened apatite crystals deteriorate mechanical properties of bone, such as ductility.

Acknowledgements We acknowledge the support from DoD/Dept. of the Army DAMD17-03-1-0556. SIH is grateful for the support from Korea Research Foundation (2004-D00318).

References

1. J.W. Hopewell, Med. Pediatr. Oncol. **41**, 208 (2003). doi:10.1002/mpo.10338
2. K.H. Szymcyk, I.M. Shapiro, C.S. Adams, Bone **34**, 148 (2004). doi:10.1016/j.bone.2003.09.003
3. V. Gilsanz, M. Carlson, T. Roe, J. Pediatr. **117**, 238 (1990). doi:10.1016/S0022-3476(05)80536-0
4. R.C. Henderson, C.D. Madsen, C. Davis, J. Pediatr. Hematol. Oncol. **18**, 367 (1996). doi:10.1097/00043426-199611000-00006
5. W.J. Howland, R.K. Loeffler, D.E. Starchman, Radiology **117**, 677 (1975)
6. P.B. Hessling, S.F. Hough, E.D. Nel, F.A. van Riet, T. Beneke, G. Wessels, Int. J. Cancer **11**, 44 (1998)
7. H.H.W. Chen, F.B. Lee, H.R. Guo, Radiother. Oncol. **62**, 239 (2002). doi:10.1016/S0167-8140(02)00002-6
8. D.H. Kohn, N.D. Sahar, J.M. Wallace, K. Golcuk, M.D. Morris, Cells Tissue Organs. doi:10.1159/000151452). Published Online: August 15, 2008
9. S. Nicolopoulos, J.M. Gonzalez-Calbert, M.P. Alonso, M.T. Gutierrez-Rios, M.I. de Frutos, M. Vallet-Regi, J. Solid State Chem. **116**, 265 (1995). doi:10.1006/jssc.1995.1212
10. A. Meldrum, L.M. Wang, R.C. Ewing, Am. Mineral. **82**, 858 (1997)
11. E.F. Bres, J.L. Hutchison, B. Senger, J.C. Voegel, R.M. Frank, Ultramicroscopy **35**, 305 (1991). doi:10.1016/0304-3991(91)90083-I
12. W. Zhang, M. Shimojo, M. Takeguchi, J. Mater. Sci. **41**, 2577 (2006). doi:10.1007/s10853-006-7783-1
13. V. Ottani, M. Raspanti, A. Ruggeri, Micron **32**, 251 (2001). doi:10.1016/S0968-4328(00)00042-1
14. V. Ziv, I. Sabanay, T. Arad, W. Traub, S. Weiner, Microsc. Res. Tech. **33**, 203 (1996). doi:10.1002/(SICI)1097-0029(19960201)33:2<203::AID-JEMT10>3.0.CO;2-Y
15. S. Weiner, T. Arad, I. Sabanay, W. Traub, Bone **20**, 509 (1997). doi:10.1016/S8756-3282(97)00053-7
16. S.I. Hong, S.K. Hong, D.H. Kohn, Nanostructural analysis of trabecular bone. J. Mater. Sci. Mater. Med. (2008), unpublished research
17. G.A. Mariotti, Calcif. Tissue Int. **42**, S47 (1993). doi:10.1007/BF01673402
18. N.D. Sahar, S.I. Hong, D.H. Kohn, Micron **36**, 617 (2005). doi:10.1016/j.micron.2005.07.006
19. A. Ascenzi, E. Bonucci, Clin. Orthop. Rel. Res. **121**, 275 (1976)
20. S.A. Reid, Anat. Embryol. (Berl.) **174**, 329 (1986). doi:10.1007/BF00698783
21. A. Ascenzi, A. Benvenuti, J. Biomech. **19**, 455 (1986). doi:10.1016/0021-9290(86)90022-9
22. M.A. Rubin, I. Jasiuk, J. Taylor, J. Rubin, T. Ganey, R.P. Apkarian, Bone **33**, 270 (2003). doi:10.1016/S8756-3282(03)00194-7
23. D.T. Cheung, N. Perelman, D. Tong, M.E. Nimni, J. Biomed. Mater. Res. **24**, 542 (1990). doi:10.1002/jbm.820240505
24. L.H.H. Olde Damink, P.J. Dijkstra, M.J.A. Van Luyn, P.B. Van Wachem, J. Biomed. Mater. Res. **29**, 149 (1995). doi:10.1002/jbm.820290203
25. A.J. Hamer, I. Stockley, R.A. Elson, J. Bone Joint Surg. **81B**, 342 (1999). doi:10.1302/0301-620X.81B2.9083
26. H. Kafantari, E. Kounadi, M. Fatouros, M. Milonakis, M. Tzaphlidou, Bone **26**, 349 (2000). doi:10.1016/S8756-3282(99)00279-3
27. C.P. Lin, B.S. Lee, S.H. Kok, W.H. Lan, Y.C. Tesng, F.H. Lin, J. Mater. Sci.: Mater. Med. **11**, 373 (2000). doi:10.1023/A:1008986008510
28. F. Watary, J. Mater. Sci. Mater. Med. **12**, 189 (2001). doi:10.1023/A:1008913828931
29. D.D. Thornburg, C.M. Wayman, Phys. Stat. Sol. (a) **15**, 449 (1973)
30. W.J. Landis, M.J. Song, A. Leith, L. McEwen, B.F. McEwen, J. Struct. Biol. **110**, 39 (1993). doi:10.1006/jsbi.1993.1003
31. F. Banhart, J. Mater. Sci. **41**, 4505 (2006). doi:10.1007/s10853-006-0081-0
32. R. Ben-Yosef, V. Soyfer, A. Vexler, Radiother. Oncol. **74**, 21 (2005). doi:10.1016/j.radonc.2004.08.019
33. B. Jeremic, B. Milicic, Radiother. Oncol. **87**, 201 (2008). doi:10.1016/j.radonc.2007.12.023
34. C. Dissanayake, Science **309**, 883 (2005). doi:10.1126/science.1115174
35. E.D. Eanes, in *Calcification in Biological Systems*, ed. by E. Bonucci (CRC Press, Boca Raton, FL, 1992), p. 1